Photodynamic inactivation of a RNA-virus model using water-soluble β-octa-Substituted pyridinium-pyrazolyl phthalocyanines

Sara R.D. Gamelas [a], Maria Bartolomeu [b], Thierry J. Gomes [b], Maria A.F. Faustino [a], João P.C. Tomé [c], Augusto C. Tomé [a], Adelaide Almeida [b], Ana T.P.C. Gomes [d,**], Leandro M. O. Lourenço [a,*]

[a] *LAQV-REQUIMTE and Department of Chemistry, University of Aveiro, 3810-193, Aveiro, Portugal*
[b] *CESAM and Department of Biology, University of Aveiro, 3810-193, Aveiro, Portugal*
[c] *CQE, Institute of Molecular Sciences, Departamento de Engenharia Química, Instituto Superior Técnico, Universidade de Lisboa, 1049–001, Lisboa, Portugal*
[d] *Universidade Católica Portuguesa, Faculty of Dental Medicine (FMD), Center for Interdisciplinary Research in Health (CIIS), 3504-505, Viseu, Portugal*

ARTICLE INFO

ABSTRACT

Among the various groups of microorganisms, viruses have generally a greater capacity for mutation, especially RNA viruses, as was demonstrated by SARS-CoV2 virus mutations. This high mutation rate promotes the development of their resistance to traditional antivirals and establishes the resistance behaviour in virus populations, decreasing their susceptibility to these drugs. In this context, the photodynamic treatment appears as a potentially effective method against microorganisms and, considering its mode of action is not likely to lead to the development of resistance. In this work, two newly zinc(II) phthalocyanines (ZnPcs) bearing pyridinium-pyrazolyl groups (**2a** and **3a**) were synthesized, characterized, and applied in photodynamic inactivation (PDI) of bacteriophage Φ6 (or Phage Phi6) as a RNA-virus model. These quaternized dyes were applied at different concentrations (from 5.0 to 20 μM, and under white light irradiation in the irradiance range between 50 and 150 mW/cm^2) to test their efficiency for possible clinical or environmental applications. The results showed that the new cationic ZnPcs **2a** and **3a** efficiently inactivate the RNA-virus model (bacteriophage Φ6), even at the lowest tested irradiance. These compounds are thus promising photosensitizers to be used in various contexts.

1. Introduction

Generically, viruses present high evolution rates, influenced by their high mutation rates [1]. Among this group of biological entities, RNA-based viruses tend to have higher mutation rates when compared to DNA-based viruses [1,2]. One of the main reasons seems to be linked to the inexistence of repair mechanisms capable of recognizing the errors introduced by the polymerase activity in the majority of RNA viruses [3], in contrast to DNA viruses. Higher mutation rates bring higher genetic variations within a population, resulting in higher viral fitness [1,4,5]. Although it is known that most mutations are deleterious, some will bring the ability to antigenic variants generation, and so the evasion of the immune system response of the host is an unquestionable advantage for the infective particles. Along with the avoidance of the neutralizing antibodies of the host organism, the design of effective

vaccines is similarly more complicated as the resultant evolution can increase the number of serotypes that circulate in human populations [6]. For mammalian RNA viruses, such as human immunodeficiency virus (HIV), influenza A, and coronavirus, the error rate can be high as 10^{-6} to 10^{-3} mutations per site per genome replication [2,7,8]. This aspect will easily increase the establishment of resistance to antiviral drugs when the community is under selective pressure [9]. Actually, antiviral drug resistance has been reported for Human viruses, such as HIV, hepatitis B, hepatitis C, herpes (HSV), and influenza A [9,10].

Photodynamic inactivation (PDI) of microorganisms has gained special attention as an alternative method to conventional treatments and has already been shown to be effective against Gram-(−) and Gram-(+) bacteria, viruses, fungi, and parasites [11–21]. Using various photosensitizers (PSs), this therapy can be applied in clinical and non-clinical contexts [22–24]. Besides PSs, the PDI approach requires

---

* Corresponding author.
** Corresponding author.
    E-mail addresses: apgomes@ucp.pt (A.T.P.C. Gomes), leandrolourenco@ua.pt (L.M.O. Lourenço).

appropriate light irradiation and molecular dioxygen (O_2). During this process, the short-lived singlet state of the PS is converted into a long-lived triplet state that allows the generation of reactive oxygen species (ROS), such as $^1O_2$, $O_2^{\bullet-}$, $OH^\bullet$, and H_2O_2 [21,25–27]. These species lead to severe oxidation of the vital constituents of the microbial structure targets [28–30].

Porphyrin [15,25,31], chlorin [15,32,33], and phthalocyanine (Pc) [26,34–36] have extensively been used as PS in PDI of microorganisms. In fact, in the last years, several free-base and metalated Pc derivatives have been synthesized with different structural features to improve their solubility and affinity to Gram-(−) bacteria, known to be less sensitive to photodynamic treatment. For this purpose, inserting suitable cationic substituents on the periphery of the Pc macrocycle is a remarkable strategy for their PDI process [26,37–43]. From this point of view, pyridinium-pyrazolyl moieties can be used to improve water solubility, as recently observed on other PSs structures used for the photo-inactivation of Gram-(−) bacteria either in planktonic or biofilm forms [15]. Moreover, the Pc dyes have adequate photophysical and photo-chemical properties to be used as PS in PDI [34,44]. Their UV–visible absorption spectra are characterized by a broad Soret band between 300 and 450 nm and by Q bands located in the red region of the spectrum (550–750 nm) [34]. Pc is being used with success in the photodynamic therapy (PDT) of cancer [45] and PDI of several microorganisms, including on surface disinfection [40,46–49].

This study evaluated the efficiency of two quaternized zinc(II) phthalocyanines in PDI of bacteriophage Φ6, as a surrogate for RNA viruses, to acknowledge their potential to be used either in clinical photodynamic treatments or environmental applications [50]. Thus, two new zinc(II) phthalocyanines bearing pyridinium-pyrazolyl groups (ZnPcs **2a** and **3a**, Scheme 1) were synthesized from the corresponding pyridine-pyrazolyl phthalocyanine derivatives (ZnPcs **2** and **3**). The PDI assays were performed with the quaternized ZnPcs **2a** and **3a** at three different concentrations (5, 10, and 20 μM) under white light irradiation (400–700 nm) at two different irradiances (50 and 150 mW/cm^2).

2. Results

2.1. Synthesis and structural characterization of ZnPc dyes

The ZnPc **2** (Scheme 1) was synthesized from the previously pre-pared phthalonitrile **1** (Pht **1**), which was prepared through a nucleophilic aromatic substitution reaction of 4,5-difluorophthalonitrile with 4-(1*H*-pyrazol-3-yl)pyridine in the presence of K_2CO_3 in a very good yield (86% yield). The structure of the Pht **1** was confirmed by ^1H and ^{13}C NMR spectroscopy (Figs. SI1 and SI2). The 2D HSQC (Fig. SI3) and HMBC (Fig. SI4) NMR spectra were also obtained to unequivocally assign the protons and carbons' resonances. Mass spectrum (Fig. SI15) also corroborated the substitution of the two fluorine atoms of the 4,5-difluorophthalonitrile by the 4-(1*H*-pyrazol-3-yl)pyridine.

The ZnPc **2** was obtained in 46% yield as a green powder through the condensation reaction of the corresponding Pht **1**, Zn(OAc)$_2$, and 1,8-diazabicyclo[5.4.0]undec-7-ene (DBU) in pentan-1-ol at 120 °C during 72 h. It was characterized by ^1H and ^{13}C NMR (Figs. SI6 and SI7), and ESI-MS (Fig. SI16).

The ZnPc **3** was obtained in 65% yield from the nucleophilic aro-matic substitution reaction of the commercially available **ZnPcF$_{16}$** with 4-(1*H*-pyrazol-3-yl)pyridine in DMF at 80 °C for 72 h. The ZnPc **3** was characterized by its ^1H, ^{19}F, and ^{13}C NMR spectra (Figs. SI7-SI9). The ^1H NMR spectrum of ZnPc **3** showed two multiplets at δ 7.22−7.88 ppm and δ 8.19−8.87 ppm, corresponding, respectively, to the resonances of the 16 *ortho*-pyridine protons, and 16 pyrazole and 16 *meta*-pyridine pro-tons. The ^{19}F NMR spectrum of ZnPc **3** (Fig. SI8) shows the signal due to the α-fluorine resonances as a singlet at δ −122.17 ppm, which confirms the substitution of all 8 β-fluorine atoms of the **ZnPcF$_{16}$** by the 4-(1*H*-pyrazol-3-yl)pyridine units.

The cationization of ZnPcs **2** and **3** was performed with an excess of methyl iodide in DMF at 40 °C for 24 h, affording the cationic derivatives ZnPc **2a** (32% yield) and ZnPc **3a** (74% yield), respectively. The catio-nization of each compound was confirmed by their ^1H NMR spectra (Figs. SI10 and SI12) with the appearance of a singlet at *ca.* δ 4.33 ppm, corresponding to the resonance of the N$^+$-CH$_3$ protons of **2a** and **3a**. The ESI-MS spectra of **2a** and **3a** (Figs. SI18 and SI19) also confirmed the pyridinium formation, exhibiting the characteristic fragmentation pathway.

2.2. Photochemical and photophysical properties

The absorption spectra of the neutral (**2** and **3**) and of the cationic phthalocyanines (**2a** and **3a**) were recorded in DMSO solutions at 298 K (Fig. 1). All ZnPcs exhibit a Soret band between 300 and 450 nm and a Q band with strong absorption between 550 and 800 nm, which are characteristic absorption features of metalated phthalocyanines. The
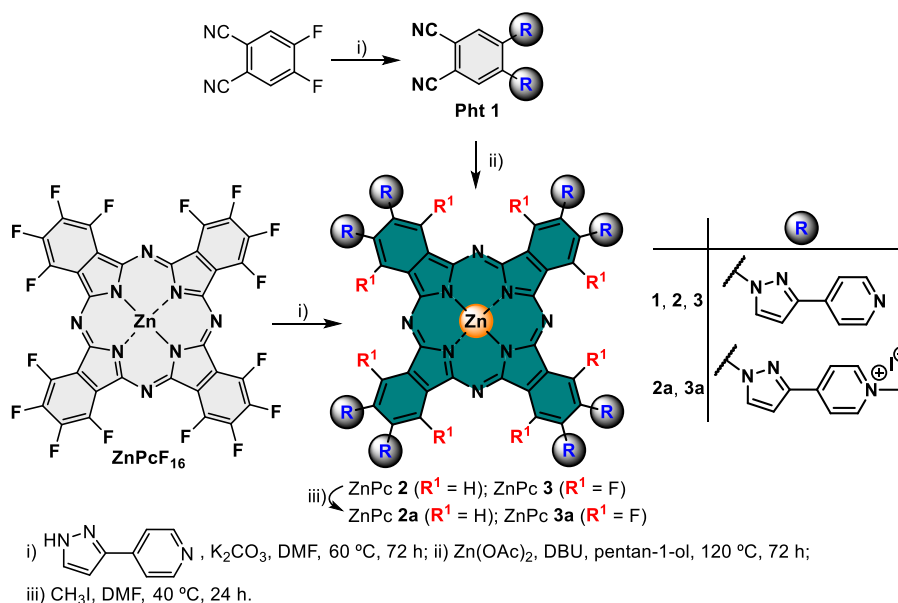
Scheme 1. Synthesis of Pht **1**, ZnPcs **2** and **3**, and quaternized ZnPcs **2a** and **3a**.
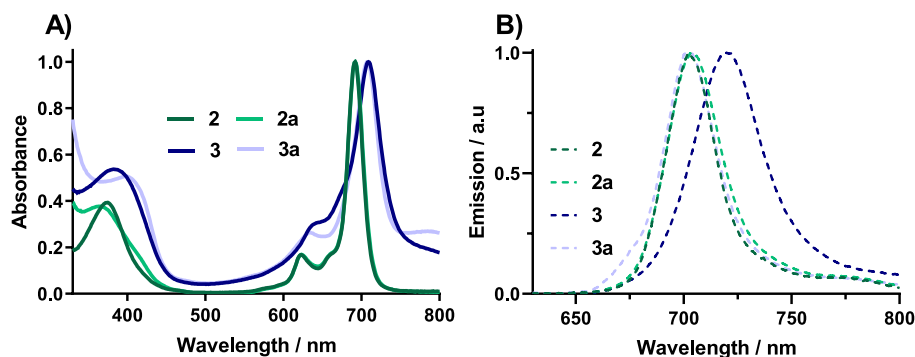
Fig. 1. Normalized A) absorption and B) emission spectra of ZnPcs **2**, **2a**, **3**, and **3a** in DMSO at 298 K ($\lambda_{exc.}$ = 620 nm).

absorption maxima for the compounds are described on Table 1. After excitation at 620 nm, ZnPcs **2**, **2a**, and **3a** showed an emission band with a maximum at 701, 702, and 704 nm, respectively, whereas ZnPc **3** showed a red-shift to 719 nm.

The photophysical features of the ZnPc derivatives as the wavelength of their Soret and Q bands, molar extinction coefficients (ε), fluorescence emission wavelength ($\lambda_{em.}$), Φ_F and Φ_Δ values and the Log $P_{o/w}$ are summarised in Table 1. The fluorescence quantum yields of the four new Pcs in DMSO are higher than that of commercial **ZnPcF$_{16}$** [51] in acetone, which was used as a reference. The neutral non-fluorinated ZnPc **2** has higher fluorescence quantum yield when compared with the neutral fluorinated ZnPc **3**, which slightly decreased after cationization. The fluorinated ZnPcs **3** and **3a** have comparable fluorescence yields to the one of **ZnPcF$_{16}$** (Φ_F = 0.04) [51]. These results were comparable to the ones in literature for Pcs with pyridine and pyridinium groups [52].

The singlet oxygen ($^1O_2$) specie is the main responsible for damaging and even inducing microbial inactivation. It is well-known that the positively charged PS and water soluble are promising photosensitizers to photoinactive microorganisms [15,25,26,31,35,53,54]. For that reason, it is important to study the ability of the cationic ZnPcs **2a** and **3a** to generate $^1O_2$. This ability was evaluated by monitoring the photooxidation of the $^1O_2$ quencher 1,3-diphenylisobenzofuran (DPiBF). In the presence of $^1O_2$, the DPiBF undertakes a [4 + 2] cycloaddition leading to the colorless 1,2-dibenzoylbenzene. Given that DPiBF absorbs at 415 nm, it is possible to monitor its absorbance decay due to the generation of $^1O_2$. The **ZnPcF$_{16}$** (Φ_Δ = 0.13) was selected as the $^1O_2$ reference. Upon irradiation at 630 nm ± 20 nm, ZnPc **2a** showed a higher capacity of $^1O_2$ generation (similar to the **ZnPcF$_{16}$**) when compared to the $^1O_2$ generation capacity of ZnPc **3a** (Φ_Δ = 0.05). This effect is consistent with other cationic phthalocyanines reported in the literature [26,55].

According to the partition coefficients between octan-1-ol and phosphate-buffer saline (PBS) solution (Log $P_{o/w}$, Table 1), ZnPc **3a** (Log $P_{o/w}$ value of 1.05) showed to be more hydrophilic than ZnPc **2a** (Log $P_{o/w}$ value of 1.58). These values are similar to those reported for other cationic phthalocyanines [56].

Considering the potential use of the ZnPcs **2a** and **3a**, the evaluation of their stability and photostability in aqueous medium is essential. The stability and photostability of ZnPc **2a** and **3a** were estimated by

monitoring the absorbance decay of their Q bands in the dark (stability) and after white (400–800 nm) light irradiation at an irradiance of 150 mW/cm^2 (photostability) – Table 2. The results showed that both cationic Pcs are stable in the dark and under white light irradiation. Both cationic ZnPcs **2a** and **3a** showed no aggregation behavior in PBS at concentrations between 0 and 25 μM (Figs. SI21).

2.3. Biological studies

The photoinactivation effect of the cationic ZnPcs **2a** and **3a** was investigated against the bacteriophage Φ6, at different concentrations (from 5.0 to 20 μM), light irradiances (50 and 150 mW/cm^2, and different total light doses from 0 to 1.08 kJ/cm^2), to investigate the most efficient conditions for these cationic ZnPc derivatives.

For each assay, light controls (LC) were performed to assess the bacteriophage Φ6 viability when the samples were irradiated with white light (400–700) (without the addition of the PS, LC), at the highest tested irradiance and light dose. Similarly, dark controls (DC) were also performed at the highest tested concentration (20 μM), for each ZnPc to evaluate their dark toxicity (Figs. SI22). The results related to the LC and DC controls showed that no significant effect was detected either by white light (LC at Fig. 2A and B, and Figs. SI23 and SI24) nor by the ZnPc **2a** and ZnPc **3a** alone (Figs. SI22), revealing that any antimicrobial effect occurring during the PDI assays was resultant of the combined action of the PSs and their activation under white light irradiation.

Overall, the effect of the compounds' concentration was noticed (Anova, $p < 0.05$), and the higher tested concentration (20 μM) lead to a higher bacteriophage Φ6 inactivation rate for both compounds **2a** and **3a**.

With the cationic compound **2a**, at an irradiance of 50 mW/cm^2 (Fig. 2A), the complete inactivation of the bacteriophage Φ6 occurred until the detection limit of the method when the compound was tested at 20 μM and after 120 min of treatment (light dose of 360 J/cm^2), with a viability reduction of >8.0 log PFU/mL (Anova, $p < 0.05$). After 60 min of light irradiation (total light dose 180 J/cm^2) at a concentration of 20 μM, the viral inactivation reaches 3.0 log of PFU/mL reduction, and the threshold to a compound can be considered a good disinfectant [57]. When tested at lower concentrations (10 and 5.0 μM), the same ZnPc **2a** promoted a bacteriophage reduction of 4.9 and 3.2 log PFU/mL (Anova, $p < 0.05$), respectively, after 120 min of light irradiation. At the concentration of 10 μM of ZnPc **2a**, 3.0 log of PFU/mL reduction was reached after 90 min of white light irradiation (total light dose of 270

Table 1
Photophysical parameters of ZnPcs **2,3** and **2a,3a** in DMSO at 298 K.

ZnPcs	Soret (nm)	Log ε	Q bands (nm)	Log ε	$\lambda_{em.}$ (nm)	Φ_F[a]	Φ_Δ[a]	Log $P_{O/W}$
2	374	5.0	692	5.4	702	0.31	n.d.	n.d.
2a	364	5.1	692	5.6	704	0.22	0.13	1.58
3	387	4.9	709	5.1	719	0.09	n.d.	n.d.
3a	398	4.8	707	5.1	701	0.03	0.05	1.05

[a] Using ZnPcF$_{16}$ as reference [51].

Table 2
Q band reduction percentage of ZnPcs **2a** and **3a** in PBS after 60 min in the dark and under white (400–800 nm) light irradiation at 150 mW/cm^2.

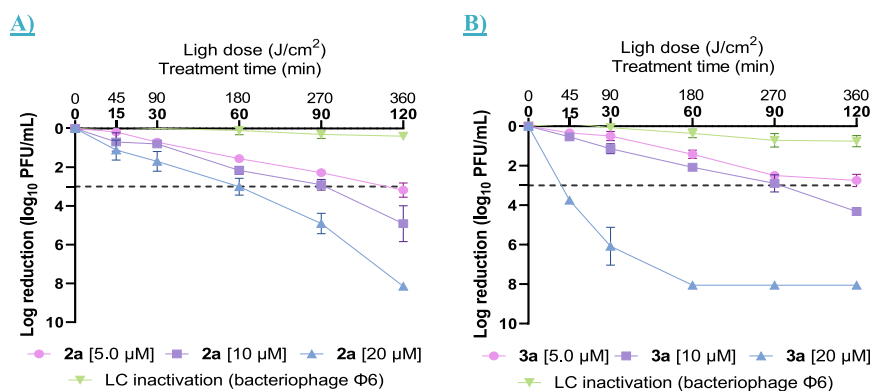| PSs	Dark (No light)	White light (400–800 nm)
2a	5.0%	0.0%
3a	0.0%	0.0%

Fig. 2. PDI of bacteriophage Φ6 using the A) ZnPc **2a** and B) ZnPc **3a** in PBS under white light exposure at 50 mW/cm^2. Treatment time (min) and respective light dose (J/cm^2) are presented on the X-axis. Data points represent the average of three independent experiments; error bars represent the standard deviation and in some cases are collapsed with the symbols; the dashed line represents the bacteriophage content 3.0 log reduction target.

J/cm^2), and for **2a** at 5.0 μM this threshold was reached after 120 min of irradiation.

The increment of light irradiance from 50 to 150 mW/cm^2 delivery by a LED system and a LUMACARE device, respectively, has not implied, in general, an increment in the photoinactivation efficiency of compound **2a** ($p > 0.05$), in the majority of experimental checkpoints (Figs. SI23).

When assessing compound **3a** (at 50 mW/cm^2) effectiveness in the inactivation of bacteriophage Φ6, a 3.0 log reduction in the bacteriophage content was reached after 90 min (270 J/cm^2) and 120 min (360 J/cm^2) when assessed at the concentrations of 10 and 5.0 μM, respectively (Fig. 2B). However, at a concentration of 20 μM, the antiviral efficiency was significantly increased ($p < 0.05$) with 3.0 log reduction reached just after 15 min (total light dose of 45 J/cm^2) and >8.0 log PFU/mL reduction achieved after 60 min (total light dose of 180 J/cm^2).

Regarding the non-significant increase in the antimicrobial activity effectiveness through light intensity increment from 50 mW/cm^2 to 150 mW/cm^2, similar behaviour was observed in ZnPc **3a** (Figs. SI24).

3. Discussion

Pyridinium-pyrazolyl groups were already used in the design of both porphyrins and chlorins to photoinactivate bacteria in their planktonic and biofilm forms, given the known behaviour as antimicrobial agents of pyrazole derivatives [15]. The present study began by synthesizing new octa-substituted phthalocyanines with those substituents. These phthalocyanines were structurally characterized, and their photophysical properties are consistent with those reported to other metalled phthalocyanines [26,34,40,41].

By testing the effect of both compounds' concentration (from 5.0 to 20 μM) at both light irradiances (50 and 150 mW/cm^2) – translating into light doses variations –, the effect of the concentration was noticed (Anova, $p < 0.05$), and the higher tested concentration (20 μM) led to a higher inactivation rate of bacteriophage Φ6 for both compounds **2a** and **3a**. The obtained results for ZnPcs **2a** and **3a** also showed good stability/solubility of the compounds in aqueous solutions, confirmed by the determined photophysical properties. However, looking in detail at the inactivation results, ZnPc **3a** showed higher inactivation capacity throughout the tested conditions, especially at 20 μM, achieving reductions >3.0 log just after 15 min of treatment (45 J/cm^2), under the lower tested irradiance intensity (50 mW/cm^2), comparing with the compound **2a**, reaching only 1.1 log reduction after 15 min of treatment. A similar behaviour was seen when the light irradiance was increased to 150 mW/cm^2 during the PDI treatments (Figs. SI23 and SI24). Since the photostability of the compounds was maintained throughout the tested light conditions (150 mW/cm^2), the non-increment of inactivation efficiency through the irradiation augmentation implies that the

excitation capacity of both compounds was already reached a light intensity of 50 mW/cm^2. So, the light increased from 50 to 150 mW/cm^2 was not translated into a PDI efficiency increment. The no correlation between the light dose at different irradiances and the photodynamic effect was already described in the literature [58].

Although ZnPc **2a** presented a higher capacity for $^1O_2$ generation, the higher antiviral behaviour demonstrated by ZnPc **3a** may have been due to the high hydrophilicity of this compound, given by the fluorine atoms.

In previous studies, it was demonstrated that RNA viruses seem to be more susceptible to photodynamic treatment than their DNA counterparts [16,17,50,59]. However, in the literature, it has been reported that the development of resistance to this antimicrobial approach by viral particles is unlikely since the photosensitization involves the generation of $^1O_2$ as well as free radical species, causing irreversible molecular damage to the viral particles in a multi-target way [17,59]. Also, the outer structures are the primary targets: particularly, structural lipids present on the viruses' envelope, sustaining the results that have been reported that enveloped viruses are more prone to be attacked by the ROS formed during photodynamic treatment [59]. Bacteriophage Φ6 is an enveloped virus of the *Cystoviridae* family, suggested as a good surrogate for enveloped RNA viruses, including SARS-CoV2, composed of a lipidic outer membrane [60]. This surrogacy is fuelled by the sharing characteristics in structure, their survival in water and sewage, and their behaviour under specific environmental conditions, making bacteriophage Φ6 a safe, excellent, and low-cost surrogate for mammalian RNA viruses, including SARS-CoV2 [61–64].

Previous studies of the photodynamic treatment of bacteriophage Φ6 using a different class of PS (a tricationic porphyrin derivative) have shown an effective inactivation of the viral particles, without the development of resistance after several cycles of photodynamic treatment cycles [65]. In addition, recent studies using a tetracationic porphyrin derivative against bacteriophage Φ6 demonstrated an effective action from this type of PSs, in different environments, such as buffered solution with controlled composition, and real wastewater as a very complex matrix [16]. Although performed against bacteria and DNA viruses, previous studies have revealed that even when the PDI treatment is performed in highly complex matrices such as wastewater, the PDI proves its robustness as an antimicrobial approach [17,66].

4. Experimental

All reagents used in this work were purchased from Merck and used directly due to their high degree of purity. The solvents were submitted to distillation and dried according to the literature [67]. Analytical thin layer chromatography (TLC) was carried out on precoated silica sheets with silica gel (Merck 60, 0.2 mm thick). Column chromatography was

carried out using silica gel (Merck, 35–70 mesh).

The ^{1}H and ^{19}F NMR spectra were recorded on a Bruker AMX 300 spectrometer at 300.13 MHz and 282.38 MHz, respectively. ^{13}C NMR spectra were recorded on a Bruker AMX 300 or Bruker AMX 500 at 75.5 MHz and 125.8 MHz, respectively. For all spectra, deuterated dimethyl sulfoxide (DMSO-d_6) was used as a solvent, and tetramethylsilane (TMS) was used as an internal reference. The chemical shifts are expressed in δ (ppm), and the coupling constants (*J*) in Hertz (Hz).

ESI-MS spectra of the compounds were recorded using Q-TOF 2 instrument (Micromass, Manchester, UK). A sample solution of 1 mg/mL was prepared by dissolving the respective compound in CH_2Cl_2 or CH_2Cl_2/MeOH (90:10). Then, a dilution of 2 μL of the solutions with 200 μL of methanol/formic acid (0.1%) was prepared for direct ESI analysis, where nitrogen was used as a nebulizer gas. The final samples were introduced into the mass spectrometer at a flow rate of 10 μL/min; the needle voltage was set at 3000 V with the ion source at 80 °C and desolvation temperature of 150 °C. The spectra were acquired for a cone voltage of 30 V, and the respective data acquisition was carried out using a Micromass MassLynx 4 data system.

The absorption spectra of ZnPcs **2,3** and **2a,3a** were recorded on a Shimadzu UV-2501-PC using dimethyl sulfoxide (DMSO) as a solvent. Steady-state fluorescence spectra of ZnPcs **2,3** and **2a,3a** were recorded on a computer-controlled Horiba Jobin Yvon FluoroMax-3 spectrofluorometer in DMSO in 1 × 1 cm quartz optical cells under normal atmospheric conditions. The fluorescence quantum yields (Φ_F) of ZnPcs **2,3** and **2a,3a** were registered between 650 and 800 nm after excitation at 620 nm with an OD of 0.05, calculated by comparing the area below the emission spectra of these derivatives with zinc(II) 1,2,3,4,8,9,10,11,15,16,17,18,22,23,24,25-hexadecafluoro-29*H*,31*H*-phthalocyanine (**ZnPcF$_{16}$**) as a standard ($\Phi_F = 0.04$ in acetone) [51].

4.1. Synthesis and characterization of precursors and photosensitizers

4.1.1. 4,5-bis[3-(pyridin-4-yl)-1H-pyrazol-1-yl]phthalonitrile, Pht 1

4,5-Difluorophthalonitrile (50.0 mg, 0.305 mmol), 4-(1*H*-pyrazol-3-yl)pyridine (90.7 mg, 0.625 mmol), and K_2CO_3 (86.7 mg, 0.625 mmol) in dry dimethylformamide (DMF) (3 mL) were left stirring for 72 h at 60 °C under N_2 atmosphere. Then, the solvent was evaporated until dry, and the reaction mixture was purified by silica column chromatography using a mixture of CH_2Cl_2/MeOH (95/5) as eluent. The obtained main fraction was precipitated from a mixture of CH_2Cl_2/MeOH (3:1) with a portion of hexane affording a white powder identified as Pht **1** (106.0 mg, 0.256 mmol) with 86% yield. ^{1}H NMR (300.13 MHz, DMSO-d_6): δ 7.21 (d, *J* = 2.7 Hz, 2H, pyrazole-H$^{2'}$), 7.70 (dd, *J* = 4.7 Hz, *J* = 1.3 Hz, 4H, Py-*o*-H), 7.92 (d, *J* = 2.7 Hz, 4H, pyrazole-H$^{1'}$), 8.57 (dd, *J* = 4.7 Hz, *J* = 1.3 Hz, 4H, Py-*m*-H), 8.77 (s, 2H, Pht-H^{3,6}) ppm. ^{13}C NMR (75.5 MHz, DMSO-d_6): δ 107.0 (C$^{2'}$), 114.7 (CN or C^{1,2}), 114.9 (CN or C^{1,2}), 119.9 (C-Py-*o*), 132.2 (C^{3,6}), 133.9 (C$^{1'}$), 136.7 (C^{4,5}), 138.9 (Py-C$^{4'}$), 150.2 (C-Py-*m*), 150.9 (C$^{3'}$) ppm. **HRMS**: *m/z* calculated for $C_{24}H_{14}N_8$: *m/z* 414.13414; found: *m/z* 415.1397 [M+H]$^+$ and *m/z* 208.0737 [M+2H]$^{2+}$.

4.1.2. Zinc(II) 2,3,9,10,16,17,23,24-octakis[3-(pyridin-4-yl)-1H-pyrazol-1-yl]phthalocyanine, 2

In a sealed tube, Pht **1** (136.7 mg, 0.330 mmol) in pentan-1-ol (2 mL) was stirred at 80 °C for 1 h. Then, Zn(OAc)$_2$ (91 mg, 0.330 mmol) and DBU (20 drops) were added and the temperature was raised to 120 °C. After 72 h, the solvent was distilled until dryness, and the obtained product was precipitated in acetone/hexane and washed with H$_2$O, CH$_2$Cl$_2$, and hexane. ZnPc **2** (65.1 mg, 0.037 mmol) was isolated in 46% yield. ^{1}H NMR (300.13 MHz, DMSO-d_6): δ 7.09–7.18 (m, 8H, pyrazole-H$^{2'}$), 7.68–7.84 (m, 24H, Py-*o*-H, and pyrazole-H$^{1'}$), 8.51–8.69 (m, 24H, Py-*m*-H, and α-H) ppm. ^{13}C NMR (125.8 MHz, DMSO-d_6): δ 105.3, 106.1, 119.4, 119.9, 134.0, 139.8, 150.2, 162.4, 174.6 ppm. **ESI-MS** (*m/z*): ESI-MS (*m/z*): 266.2 [M + 4H + K - 3PyrPy]$^{5+}$ (blue circle), 338.5 [M + 2H + Na + K - 3PyrPy]$^{4+}$, 378.3 [M + 2H + 2K - 2PyrPy]$^{4+}$, 394.5 [M + 4H - PyrPy]$^{4+}$, 453.9 [M + H + 2K -3PyrPy]$^{3+}$, 548.5 [M + H + Na + K - PyrPy]$^{3+}$, 574.5 [M + 3H]$^{3+}$ (yellow circle), 581.5 [M + 2H + Na]$^{3+}$, and 861.9 [M + 2H]$^{2+}$. **UV–Vis** (DMF), $\lambda_{max.}$ (log ε): 374 (5.0), 622 (4.7), 692 (5.4) nm. Fluorescence quantum yield (Φ_F) in DMSO: $\Phi_F = 0.31$.

4.1.3. Zinc(II) 1,4,8,11,15,18,22,25-octafluoro-2,3,9,10,16,17,23,24-octakis[3-(pyridin-4-yl)-1H-pyrazol-1-yl]phthalocyanine, 3

Commercial available perfluorinated phthalocyaninatozinc(II) (**ZnPcF$_{16}$**) (100.0 mg, 0.116 mmol), 4-(1*H*-pyrazol-3-yl)pyridine (135.0 mg, 0.930 mmol), K_2CO_3 (128.5 mg, 0.930 mmol) and DMF (3 mL) were added to a bottom rounded flask and the reaction mixture was kept under a nitrogen atmosphere for 72 h at 60 °C. After the complete reaction, the solvent was distilled until dry. The product was precipitated in acetone/hexane and washed several times with H$_2$O, CH$_2$Cl$_2$, and hexane. The obtained product ZnPc **3** (187.5 mg, 0.100 mmol) was isolated as a blue powder in 65% yield. ^{1}H NMR (300.13 MHz, DMSO-d_6): δ 7.22–7.88 (m, 16H, Py-*o*-H), 8.19–8.87 (m, 32H, pyrazole-H$^{2'}$, Py-*m*-H and pyrazole-H$^{1'}$) ppm. ^{19}F NMR (282.38 MHz, DMSO-d_6): δ −122.17 (s, 8F, Ar-F) ppm. ^{13}C NMR (125.8 MHz, DMSO-d_6): δ 105.4, 105.7, 106.0, 119.9, 136.0, 136.2, 139.4, 149.0, 150.0, 150.8, 151.3, 156.3 ppm. **ESI-MS** (*m/z*): 272.2 [M + 6H + K]$^{7+}$, 360.8 [M + 4H - 3PyrPy]$^{4+}$, 454.0 [M + H + 2K - 4PyrPy]$^{3+}$, 530.1 [M + Na + K - 6PyrPy]$^{2+}$, 594.2 [M + Na + K - PyrPy]$^{2+}$ (blue circle), 622.7 [M + 3H]$^{3+}$ (yellow circle), and 933.9 [M + 2H]$^{2+}$. **UV–Vis** (DMF), $\lambda_{max.}$ (log ε): 387 (4.9), 645 (4.6), 709 (5.1) nm. Fluorescence quantum yield in DMSO: $\Phi_F = 0.09$.

4.1.4. Zinc(II) 2,3,9,10,16,17,23,24-octakis[3-(1-methylpyridinium-4-yl)-1H-pyrazol-1-yl]phthalocyanine octaiodide, 2a

In a sealed tube, the ZnPc **2** (60.0 mg, 0.0035 mmol) and an excess of methyl iodide (1 mL, 0.32 mmol) were mixed in DMF (2 mL). The reaction mixture was kept at 40 °C for 24 h and, then precipitated in CH$_2$Cl$_2$, filtered, and washed with water. ZnPc **2a** (32.0 mg, 0.0012 mmol) was isolated as a green powder in 32% yield. ^{1}H NMR (300.13 MHz, DMSO-d_6): δ 4.34 (s, 24H, –CH$_3$), 7.64 (d, *J* = 2.5 Hz, 8H, pyrazole-H$^{2'}$), 8.50 (d, *J* = 6.9 Hz, 16H, Py-*o*-H), 8.60 (d, *J* = 2.5 Hz, 8H, pyrazole-H$^{1'}$), 9.02 (d, *J* = 6.9 Hz, 16H, Py-*m*-H), 10.03 (s, 8H, α-H) ppm. ^{13}C NMR (125.8 MHz, DMSO-d_6): δ 47.3, 108.4, 121.6, 122.4, 122.7, 135.7, 135.8, 138.3, 138.4, 145.9, 146.5, 147.4, 153.0 ppm. **ESI-MS** (*m/z*): 272.2 [M^{8+} + 3e$^-$ + Na + K]$^{7+}$, 324.3 [M^{8+} + I - CH$_3$]$^{6+}$, 338.5 [M^{8+} + 3e$^-$ + I + K + Na]$^{6+}$ (blue circle), 368.9 [M^{8+} + 3e$^-$]$^{5+}$, 452.0 [M^{8+} + 2 e$^-$ - 2CH$_3$]$^{4+}$, 460.1 [M^{8+} + 4e$^-$]$^{4+}$ (yellow circle), 631.1 [M^{8+} + I + H - 5CH$_3$]$^{3+}$, and 672.4 [M^{8+} + 2I + 2H - 5CH$_3$]$^{3+}$. **UV–Vis** (DMF), $\lambda_{max.}$ (log ε): 364 (5.1), 623 (4.8), 692 (5.6) nm. Fluorescence quantum yield in DMSO, $\Phi_F = 0.22$.

4.1.5. Zinc(II) 1,4,8,11,15,18,22,25-octafluoro-2,3,9,10,16,17,23,24-octakis[3-(1-methylpyridinium-4-yl)-1H-pyrazol-1-yl]phthalocyanine octaiodide, 3a

In a sealed tube, ZnPc **3** (71.7 mg, 0.038 mmol) and an excess of methyl iodide (2 mL, 32.1 mmol) were mixed in DMF (2 mL) stirring for 24 h at 40 °C. Then, the reaction mixture was directly precipitated in CH$_2$Cl$_2$, filtered, and washed with water. The ZnPc **3a** (85.6 mg, 0.029 mmol) was obtained as a green powder in 74% yield. ^{1}H NMR (300.13 MHz, DMSO-d_6): δ 4.32 (s, 24H, –CH$_3$), 7.46–7.76 (m, 8H, pyrazole-H$^{2'}$), 8.15–8.87 (m, 24H, Py-*o*-H and pyrazole-H$^{1'}$), 8.91–9.09 (m, 16H, Py-*m*-H) ppm. ^{19}F NMR (282.38 MHz, DMSO-d_6): δ −121.65 (s, 8F, Ar-F) ppm. ^{13}C NMR (125.8 MHz, DMSO-d_6): δ 47.5, 105.6, 108.2, 122.6, 134.6, 136.4, 137.9, 145.8, 146.1, 148.0, 163.3 ppm. **ESI-MS** (*m/z*): 325.2 [M^{8+} - 2CH$_3$]$^{6+}$, 338.5 [M^{8+} + 3e$^-$ + K]$^{6+}$, 396.8 [M^{8+} + 3e$^-$]$^{5+}$ (blue circle), 453.9 [M^{8+} + 2I + 2K - 3CH$_3$]$^{5+}$, 496.1 [M^{8+} + 4e$^-$]$^{4+}$ (yellow circle), 678.4 [M^{8+} + I + H - 5CH$_3$]$^{3+}$, and 720.3 [M^{8+} + 2I + 2H - 5CH$_3$]$^{3+}$. **UV–Vis** (DMF), $\lambda_{max.}$ (log ε): 398 (4.8), 634 (4.5), 707 (5.1) nm. Fluorescence quantum yield in DMSO: $\Phi_F = 0.03$.

4.2. Singlet oxygen generation

The ability to generate $^1O_2$ species of the cationic derivatives **2a** and **3a** was evaluated by monitoring the absorption of the photooxidation of 1,3-diphenylisobenzofuran (DPiBF) and using **ZnPcF$_{16}$** as a reference ($\Phi_\Delta = 0.13$ in acetone) [51]. Solutions of the cationic PSs in DMF (Abs$_{630}$ ~ 0.20) were irradiated in quartz cuvettes under aerobic conditions with a LED array composed of a matrix of 5×5 LED (total of 25 light sources) with an emission peak centered at 630 nm $\pm$ 20 nm and an irradiance of 11 mW/cm^2. The absorbance decay of DPiBF at 415 nm was measured with 30 s irradiation intervals of up to 300 s. The kinetics of the DPiBF photooxidation in the absence of any compound in DMF was also assessed, and no significant photodegradation was observed under light conditions. The results are expressed as mean and standard deviation from three independent experiments. Furthermore, the singlet oxygen quantum yields (Φ_Δ) were determined by the equation indicated below:

$$\Phi_\Delta = \Phi_\Delta^{ref} \frac{K_{sample}}{K_{ref}} \frac{1 - 10^{-Abs_{ref}}}{1 - 10^{-Abs_{sample}}}$$

Where Φ_Δ^{ref} is the singlet oxygen quantum yield of **ZnPcF$_{16}$**, K_{sample} and K_{ref} are the photodecay constant of DPiBF in the presence of the sample and the reference, respectively; Abs_{sample} and Abs_{ref} are the absorbance of the sample and the reference at 630 nm.

4.3. Determination of log P

The values of the logarithmic partition coefficients of octan-1-ol/water (log P$_{o/w}$) of ZnPcs **2a** and **3a** were determined from the experimental protocol published [68]. Stock solutions of these PSs were prepared at a concentration of 500 μM in DMSO. Then, PBS (400 μL) and octan-1-ol (400 μL) were mixed in an Eppendorf, and the stock solution of each sample (200 μL) was added. The mixture was inserted in a vortex for 5 min at r.t. and then centrifuged (10 000 rpm, 10 min, r.t.). Then, the octan-1-ol and aqueous phases were separated (the middle part between layers was tossed), and 50 μL of each layer was diluted into DMSO (2 mL). Emission spectra ($\lambda_{exc.} = 620$ nm) of the DMSO solutions containing ZnPcs **2a** and **3a** were obtained, and the log P was calculated as follows: log P = log (A$_O$/A$_{PBS}$), where A$_O$ and A$_{PBS}$ are integrated areas of the emission spectra from the DMSO solution from octan-1-ol/PBS (water) layers, respectively [68].

4.4. Stability and photostability

PBS solutions of the PSs (**2a** and **3a**) were freshly prepared in quartz cuvettes, and the respective absorbances at the Q band were adjusted to ~0.2–0.3 (concentration range of 0.5–1 μM). Then, each solution was irradiated under white light at an irradiance of 150 mW/cm^2, and the absorbance at the correspondent Q band was registered before (time t$_0$ = Abs$_0$) and after light irradiation (Abs$_t$) up to 60 min (total light dose of 1.08 kJ/cm^2):

$$Photostability\ (\%) = \left(\frac{Abs_t}{Abs_0} \right) \times 100$$

The white light irradiation an irradiance of 150 mW/cm^2 was delivered by a LumaCare system (USA, model LC122) equipped with a 250 W halogen lamp and an optical fiber with a transmittance between 400 and 800 nm.

Similar experiments were performed to determine the stability studies of the PS solutions of **2a** and **3a** without light irradiation. In this case, the cuvettes were kept dark during all the experimental periods.

4.5. Biological studies

The PDI assays were carried out with bacteriophage Φ6 as a surrogate model of enveloped RNA viruses.

4.5.1. Bacteriophage preparation and bacterial strain and growth conditions

Biological entities, bacteriophage Φ6 DSM 21518 and its bacterial host *Pseudomonas* sp. DSM 21482 was purchased from DSMZ (Deutsche Sammlung von Mikroorganismen und Zellkulturen GmbH, Braunschweig, Germany). Enriched phage stock was maintained in SM buffer [0.1 M NaCl, 8.0 mM MgSO$_4$, 20 mM Tris-HCl (reagents purchased from Sigma, St. Louis, MO, USA), 2% (w/v) gelatin, pH 7.5] and the phage titer (10^8–10^9 plate forming units per mL, PFU/mL) was determined as previously described in the literature [16]. The phage stock solution was maintained at 4 °C. *Pseudomonas* sp. cells were stored in glycerol stocks at −80 °C, and before each assay, a bacterial stock was transferred into a flask of fresh Tryptic Soy Broth (TSB, Liofilchem, Italy) and incubated for 16–18 h at 25 °C, with orbital shaking (120 rpm).

4.5.2. Photodynamic inactivation procedure

4.5.2.1. Photosensitizers.
The phthalocyanine-based PSs bearing 1-methylpyridinium-pyrazolyl groups (**2a** and **3a**) were tested on bacteriophage Φ6 PDI, used as a surrogate virus for enveloped RNA viruses. DMSO stock solutions of the used PSs were prepared at a concentration of 500 μM, maintained in the dark, and refrigerated at 4 °C until further use. Before each assay, the PSs stock solutions were brought to room temperature and sonicated for 5 min to ensure the homogeneity of the solution, and the proper volumes of the stock solution were calculated for the PSs to be tested at the concentrations of 5.0, 10, and 20 μM.

4.5.2.2. Irradiation conditions.
For the PDI assays, two white light sources with different irradiance outputs were used to determine the influence of this parameter in the inactivation rate of the tested PSs: a white (400–700 nm) light-emitting diode (LED) system (EL®MARK, 20 W, 1400 lm, 5500 K) was used at a constant irradiance of 50 mW/cm^2, or through a white (400–800 nm) light delivered from a quartz/halogen lamp (LumaCare®, USA, model LC122) used at a constant irradiance of 150 mW/cm^2. During the preparation of each assay, the irradiances were adjusted with a power meter FieldMaxII-Top combined with a Coherent PowerSens PS19Q energy sensor (Coherent, Santa Clara, CA, USA).

4.5.2.3. PDI assays.
PDI assays were performed in PBS, to which a proper volume of phage stock solution was added to achieve a phage concentration of circa 10^8 PFU/mL. The PSs **2a** and **3a** were added to the samples at different concentrations (5.0, 10, and 20 μM), and the samples were maintained in the dark for 10 min, with stirring, to promote the binding of PS to the viral particles and the homogeneity of the reactional suspension. During the experiments, the samples were maintained under magnetic stirring, and aliquots of 100 μL of samples and controls were taken at times 0, 15, 30, 60, 90, and 120 min, serially diluted in PBS and plated by the drop plated method in Petri dishes. The Petri dishes were previously prepared with TSA and a layer of TSA-soft with the phage host *Pseudomonas* sp. for monitoring the phage survival. Along with the samples, appropriate dark and light controls were performed to ensure that the PSs did not present dark toxicity to the viral particles (dark controls) or that the light alone did not interfere with the viral viability (light controls). At least three independent assays were performed for each condition in duplicate.

4.6. Statistical analysis

Statistical analysis was performed using the GraphPad Prism software program. The Kolmogorov–Smirnov test was used to check the data's normal distribution, and the homogeneity of variances was tested with the Brown–Forsythe test. ANOVA and Tukey's multiple

comparisons test were applied to assess the significance of the differences among the tested conditions of concentrations, light doses, and the respective controls. Differences corresponding to $p < 0.05$ were considered significant. Three independent assays were performed for each condition in duplicate.

5. Conclusions

Novel neutral zinc(II) phthalocyanines (**2** and **3**) and the corresponding quaternized derivatives (**2a** and **3a**) were prepared and structurally characterized by NMR, absorption, and emission spectroscopies, as well as by mass spectrometry. The photophysical measurements showed that cationic PS **2a** and **3a** are stable and photostable under white light irradiation. The non-fluorinated derivative **2a** has a higher fluorescence quantum yield ($\Phi_F = 0.22$) when compared to the fluorinated analogue **3a** ($\Phi_F = 0.03$) but both PS are able to generate singlet oxygen.

Although both cationic PS were effective against the bacteriophage Φ6 under the tested conditions, **3a** demonstrated a higher bacteriophage inactivation ability, particularly under either lower concentrations or lower light doses.

The low light irradiance needed to activate these PSs (50 mW/cm^2) allows its use in the clinical field and the environment, even at low PS concentrations (5.0 μM), highlighting PDI in the fight against RNA viruses.

Funding

CRediT authorship contribution statement

Sara R.D. Gamelas: Methodology, Validation, Investigation, Writing – original draft, Writing – review & editing. **Maria Bartolomeu:** Methodology, Validation, Investigation, Supervision, Validation, Writing – original draft, Writing – review & editing. **Thierry J. Gomes:** Methodology, Investigation. **Maria A.F. Faustino:** Validation, Resources, Writing – review & editing. **João P.C. Tomé:** Writing – review & editing, Validation, Supervision. **Augusto C. Tomé:** Writing – review & editing, Validation, Supervision. **Adelaide Almeida:** Validation, Resources, Supervision, Funding acquisition, Writing – review & editing. **Ana T.P.C. Gomes:** Conceptualization, Writing – review & editing. **Leandro M.O. Lourenço:** Conceptualization, Validation, Resources, Supervision, Funding acquisition, Writing – review & editing, All authors have read and agreed to the published version of the manuscript.

Declaration of competing interest

The authors do not have any conflict of interest with the elaboration of the scientific document and all information described was confirmed in the literature.

Data availability

Data will be made available on request.

Appendix A. Supplementary data

Supplementary data to this article can be found online at https://doi.org/10.1016/j.dyepig.2023.111661.

References

[1] Peck KM, Lauring AS. Complexities of viral mutation rates. J Virol 2018;92: e01031-17. https://doi.org/10.1128/JVI.01031-17.

[2] Cann AJ. Genomes. In: Principles of molecular virology. Elsevier; 2012. p. 55–101. ISBN 9780123849397.

[3] Barr JN, Fearns R. Genetic instability of RNA viruses. In: Genome stability. Elsevier; 2016. p. 21–35. ISBN 9780128033456.

[4] Payne S. Virus evolution and genetics. In: Viruses. Elsevier; 2017. p. 81–6. ISBN 9780128031094.

[5] Wargo AR, Kurath G. Viral fitness: definitions, measurement, and current insights. Curr Opin Virol 2012;2:538–45. https://doi.org/10.1016/j.coviro.2012.07.007.

[6] Stern A, Andino R. Viral evolution. In: Viral pathogenesis. Elsevier; 2016. p. 233–40. ISBN 9780128009642.

[7] Burrell CJ, Howard CR, Murphy FA. Pathogenesis of virus infections. In: Fenner and white's medical virology. Elsevier; 2017. p. 77–104. ISBN 9780123751560.

[8] Petrova VN, Russell CA. The evolution of seasonal influenza viruses. Nat Rev Microbiol 2018;16:47–60. https://doi.org/10.1038/nrmicro.2017.118.

[9] Kumar M, Kuroda K, Dhangar K, Mazumder P, Sonne C, Rinklebe J, Kitajima M. Potential emergence of antiviral-resistant pandemic viruses via environmental drug exposure of animal reservoirs. Environ Sci Technol 2020;54:8503–5. https://doi.org/10.1021/acs.est.0c03105.

[10] Irwin KK, Renzette N, Kowalik TF, Jensen JD. Antiviral drug resistance as an adaptive process. Virus Evol 2016;2:1–10. https://doi.org/10.1093/ve/vew014.

[11] Hamblin MR. Antimicrobial photodynamic inactivation: a bright new technique to kill resistant microbes. Curr Opin Microbiol 2016;33:67–73. https://doi.org/10.1016/j.mib.2016.06.008.

[12] Huang L, Dai T, Hamblin MR. Antimicrobial photodynamic inactivation and photodynamic therapy for infections. Methods Mol Biol 2010;635:155–73.

[13] Sousa V, Gomes ATPCP, Freitas A, Faustino MAFF, Neves MGPM, Almeida A. Photodynamic inactivation of Candida albicans in blood plasma and whole blood. Antibiotics 2019;8:221. https://doi.org/10.3390/antibiotics8040221.

[14] Rocha DMGC, Venkatramaiah N, Gomes MC, Almeida A, Faustino MAF, Almeida Paz FA, Cunha Á, Tomé JPC. Photodynamic inactivation of Escherichia coli with cationic ammonium Zn(ii) phthalocyanines. Photochem Photobiol Sci 2015;14: 1872–9. https://doi.org/10.1039/c5pp00147a.

[15] Santos I, Gamelas SRD, Vieira C, Faustino MAF, Tomé JPC, Almeida A, Gomes ATPC, Lourenço LMO. Pyrazole-pyridinium porphyrins and chlorins as powerful photosensitizers for photoinactivation of planktonic and biofilm forms of E. Coli. Dyes Pigments 2021;193:109557. https://doi.org/10.1016/j.dyepig.2021.109557.

[16] Gomes M, Bartolomeu M, Vieira C, Gomes ATPC, Faustino MAF, Neves MGPMS, Almeida A. Photoinactivation of phage Phi6 as a SARS-CoV-2 model in wastewater: evidence of efficacy and safety. Microorganisms 2022;10. https://doi.org/10.3390/microorganisms10030659.

[17] Bartolomeu M, Oliveira C, Pereira C, Neves MGPMS, Faustino MAF, Almeida A. Antimicrobial photodynamic approach in the inactivation of viruses in wastewater: influence of alternative adjuvants. Antibiotics 2021;10:767. https://doi.org/10.3390/antibiotics10070767.

[18] Wiehe A, O`brien JM, Senge MO. Trends and targets in antiviral phototherapy. Photochem Photobiol Sci 2019;18:2565–612. https://doi.org/10.1039/c9pp00211a.

[19] Nguyen VN, Zhao Z, Tang BZ, Yoon J. Organic photosensitizers for antimicrobial phototherapy. Chem Soc Rev 2022:3324–40. https://doi.org/10.1039/d1cs00647a.

[20] Ran B, Wang Z, Cai W, Ran L, Xia W, Liu W, Peng X. Organic photo-antimicrobials: principles, molecule design, and applications. J Am Chem Soc 2021;143: 17891–909. https://doi.org/10.1021/jacs.1c08679.

[21] Ruiz-González R, Setaro F, Gulías Ò, Agut M, Hahn U, Torres T, Nonell S. Cationic phthalocyanine dendrimers as potential antimicrobial photosensitisers. Org Biomol Chem 2017;15:9008–17. https://doi.org/10.1039/c7ob02270k.

[22] Ali W, Zhang H, Wang Z, Chang C, Javed A, Ali K, Du W, Niazi NK, Mao K, Yang Z. Occurrence of various viruses and recent evidence of SARS-CoV-2 in wastewater systems. J Hazard Mater 2021;414:125439. https://doi.org/10.1016/j.jhazmat.2021.125439.

[23] Serra-Compte A, González S, Arnaldos M, Berlendis S, Courtois S, Loret JF, Schlosser O, Yáñez AM, Soria-Soria E, Fittipaldi M, et al. Elimination of SARS-CoV-2 along wastewater and sludge treatment processes. Water Res 2021:202. https://doi.org/10.1016/j.watres.2021.117435.

[24] Maisch T. Photoantimicrobials—an update. Transl Biophotonics 2020;2:1–9. https://doi.org/10.1002/tbio.201900033.

[25] Calmeiro JMD, Gamelas SRD, Gomes ATPC, Faustino MAF, Neves MGPMS, Almeida A, Tomé JPC, Lourenço LMO. Versatile thiopyridyl/pyridinone porphyrins combined with potassium iodide and thiopyridinium/methoxypyridinium porphyrins on E. Coli photoinactivation. Dyes Pigments 2020;181:108476. https://doi.org/10.1016/j.dyepig.2020.108476.

[26] Gamelas SRD, Gomes ATPC, Faustino MAF, Tomé AC, Tomé JPC, Almeida A, Lourenço LMO. Photoinactivation of Escherichia coli with water-soluble ammonium-substituted phthalocyanines. ACS Appl Bio Mater 2020;3:4044–51. https://doi.org/10.1021/acsabm.0c00128.

[27] Plaetzer K, Krammer B, Berlanda J, Berr F, Kiesslich T. Photophysics and photochemistry of photodynamic therapy: fundamental aspects. Laser Med Sci 2009;24:259–68. https://doi.org/10.1007/s10103-008-0539-1.

[28] Ardiansah BA. Recent update: antimicrobial agents containing pyrazole nucleus. Asian J Pharmaceut Clin Res 2018;11:88. https://doi.org/10.22159/ajpcr.2018.v11i12.29418.

[29] Hamblin MR, Abrahamse H. Can light-based approaches overcome antimicrobial resistance? Drug Dev Res 2019;80:48–67. https://doi.org/10.1002/ddr.21453.

[30] Kashef N, Huang Y-Y, Hamblin MR. Advances in antimicrobial photodynamic inactivation at the nanoscale. Nanophotonics 2017;6:853–79. https://doi.org/10.1515/nanoph-2016-0189.

[31] Ribeiro CPS, Gamelas SRD, Faustino MAF, Gomes ATPC, Tomé JPC, Almeida A, Lourenço LMO. Unsymmetrical cationic porphyrin-cyclodextrin bioconjugates for photoinactivation of Escherichia coli. Photodiagnosis Photodyn Ther 2020;31:101788. https://doi.org/10.1016/j.pdpdt.2020.101788.

[32] Sierra-Garcia IN, Cunha Â, Lourenço LMO. In vitro photodynamic treatment of Fusarium oxysporum conidia through the action of thiopyridinium and methoxypyridinium chlorins. J Photochem Photobiol Chem 2022;432:114081. https://doi.org/10.1016/j.jphotochem.2022.114081.

[33] Calmeiro JMD, Dias CJ, Ramos CIV, Almeida A, Tomé JPC, Faustino MAF, Lourenço LMO. Comparative photodynamic inactivation of bioluminescent E. Coli by pyridinium and inverted pyridinium chlorins. Dyes Pigments 2020;173:107410. https://doi.org/10.1016/j.dyepig.2019.03.021.

[34] Ribeiro CPS, Lourenço LMO. Overview of cationic phthalocyanines for effective photoinactivation of pathogenic microorganisms. J Photochem Photobiol C Photochem Rev 2021;48:100422. https://doi.org/10.1016/j.jphotochemrev.2021.100422.

[35] Gamelas SRD, Vieira C, Bartolomeu M, Faustino MAF, Tomé JPC, Tomé AC, Almeida A, Lourenço LMO. Photodynamic inactivation of pathogenic gram-negative and gram-positive bacteria mediated by Si(IV) phthalocyanines bearing axial ammonium units. J Photochem Photobiol, B 2022;233:112502. https://doi.org/10.1016/j.jphotobiol.2022.112502.

[36] Gamelas SRD, Sierra-Garcia IN, Tomé AC, Cunha Â, Lourenço LMO. In vitro photoinactivation of Fusarium oxysporum conidia with light-activated ammonium phthalocyanines. Int J Mol Sci 2023;24:3922. https://doi.org/10.3390/ijms24043922.

[37] Ion R-M. Porphyrins and phthalocyanines: photosensitizers and photocatalysts. In: Ylmaz Y, editor. Phthalocyanines and some current applications, vol. 9. London: InTech; 2017. p. 189–221. ISBN 9789537619343.

[38] Grüner MC, Niemann S, Faust A, Strassert CA. Axially decorated SiIV-phthalocyanines bearing mannose- or ammonium-conjugated siloxanes: comparative bacterial labeling and photodynamic inactivation. Photochem Photobiol 2018;94:890–9. https://doi.org/10.1111/php.12881.

[39] Sen P, Sindelo A, Mafukidze DM, Nyokong T. Synthesis and photophysicochemical properties of novel axially di-substituted silicon (IV) phthalocyanines and their photodynamic antimicrobial chemotherapy (PACT) activity against Staphylococcus aureus. Synth Met 2019;258:116203. https://doi.org/10.1016/j.synthmet.2019.116203.

[40] Lourenço LMO, Sousa A, Gomes MC, Faustino MAF, Almeida A, Silva AMS, Neves MGPMS, Cavaleiro JAS, Cunha Â, Tomé JPC. Inverted methoxypyridinium phthalocyanines for PDI of pathogenic bacteria. Photochem Photobiol Sci 2015;14:1853–63. https://doi.org/10.1039/c5pp00145e.

[41] Lourenço LMO, Rocha DMGC, Ramos CIV, Gomes MC, Almeida A, Faustino MAF, Almeida Paz FA, Neves MGPMS, Cunha Â, Tomé JPC. Photoinactivation of planktonic and biofilm forms of Escherichia coli through the action of cationic zinc (II) phthalocyanines. ChemPhotoChem 2019;3:251–60. https://doi.org/10.1002/cptc.201900020.

[42] Merchat M, Bertolini G, Giacomini P, Villanueva A, Jori G. Meso-substituted cationic porphyrins as efficient photosensitizers of gram-positive and gram-negative bacteria. J Photochem Photobiol, B 1996;32:153–7. https://doi.org/10.1016/1011-1344(95)07147-4.

[43] Minnock A, Vernon DI, Schofield J, Griffiths J, Parish JH, Brown SB. Photoinactivation of bacteria. Use of a cationic water-soluble zinc phthalocyanine to photoinactivate both gram-negative and gram-positive bacteria. J Photochem Photobiol, B 1996;32:159–64. https://doi.org/10.1016/1011-1344(95)07148-2.

[44] Dent CE, Linstead RP, Lowe AR. Phthalocyanines. Part VI. The structure of the phthalocyanines. J Chem Soc 1934:1033. 217.

[45] Castro KADF, Prandini JA, Biazzotto JC, Tomé JPC, da Silva RS, Lourenço LMO. The surprisingly positive effect of zinc-phthalocyanines with high photodynamic therapy efficacy of melanoma cancer. Front Chem 2022;10:1–9. https://doi.org/10.3389/fchem.2022.825716.

[46] Marciel L, Teles L, Moreira B, Pacheco M, Lourenço LMO, Neves MGPMS, Tomé JPC, Faustino MAF, Almeida A. An effective and potentially safe blood disinfection protocol using tetrapyrrolic photosensitizers. Future Med Chem 2017;9:365–79. https://doi.org/10.4155/fmc-2016-0217.

[47] Lourenço LMO, Pereira PMR, Maciel E, Válega M, Domingues FMJ, Domingues MRM, Neves MGPMS, Cavaleiro JAS, Fernandes R, Tomé JPC. Amphiphilic phthalocyanine-cyclodextrin conjugates for cancer photodynamic therapy. Chem Commun 2014;50:8363–6. https://doi.org/10.1039/c4cc02226b.

[48] Revuelta-Maza MÁ, Mascaraque M, González-Jiménez P, González-Camuñas A, Nonell S, Juarranz Á, de la Torre G, Torres T. Assessing amphiphilic ABAB Zn(II) phthalocyanines with enhanced photosensitization abilities in in vitro photodynamic therapy studies against cancer. Molecules 2020;25:213.

[49] Lo PC, Rodríguez-Morgade MS, Pandey RK, Ng DKP, Torres T, Dumoulin F. The unique features and promises of phthalocyanines as advanced photosensitisers for photodynamic therapy of cancer. Chem Soc Rev 2020;49:1041–56.

[50] Costa L, Tomé JPC, Neves MGPMS, Tomé AC, Cavaleiro JAS, Cunha Â, Faustino MAF, Almeida A. Susceptibility of non-enveloped DNA- and RNA-type viruses to photodynamic inactivation. Photochem Photobiol Sci 2012;11:1520–3. https://doi.org/10.1039/c2pp25156f.

[51] Beveridge AC, Bench BA, Gorun SM, Diebold GJ. Evaluation of photodynamic therapy agents through transient grating measurements. J Phys Chem A 2003;107:5138–43. https://doi.org/10.1021/jp022646e.

[52] Joseph J, Lourenço LMO, Tomé JPC, Torres T, Guldi DM. Unique multiphthalocyanine coordination systems: vibrationally hot excited states and charge transfer states that power high energy triplet charge separated states. Nanoscale 2022. https://doi.org/10.1039/D2NR03721A.

[53] Ndemueda A, Pereira I, Faustino MAF. Cunha photodynamic inactivation of the phytopathogenic bacterium xanthomonas citri subsp. Citri. Lett Appl Microbiol 2020;71:420–7. https://doi.org/10.1111/lam.13350.

[54] Ribeiro CPS, Faustino MAF, Almeida A, Lourenço LMO. The antimicrobial photoinactivation effect on Escherichia coli through the action of inverted cationic porphyrin–cyclodextrin conjugates. Microorganisms 2022;10:1–13. https://doi.org/10.3390/microorganisms10040718.

[55] Prandini JA, Castro KADF, Biazzotto JC, Brancini GTP, Tomé JPC, Lourenço LMO, Braga GÚL, da Silva RS. Thiopyridinium phthalocyanine for improved photodynamic efficiency against pathogenic fungi. J Photochem Photobiol, B 2022;231:1–8. https://doi.org/10.1016/j.jphotobiol.2022.112459.

[56] Chiti G, Dei D, Fantetti L, Roncucci G. In vitro photosensitizing efficacy of cationic phthalocyanine derivatives against C. Albicans: effect of serum albumins. J Porphyr Phthalocyanines 2005;9:463–9. https://doi.org/10.1142/S1088424605000575.

[57] United States environmental protection agency EPA United States environmental protection agency. Pesticide Registration - Guidance for Products Adding Residual Efficacy Claims.

[58] Costa L, Carvalho CMB, Faustino MAF, Neves MGPMS, Tomé JPC, Tomé AC, Cavaleiro J a S, Cunha A, Almeida A. Sewage bacteriophage inactivation by cationic porphyrins: influence of light parameters. Photochem Photobiol Sci 2010;9:1126–33. https://doi.org/10.1039/c0pp00051e.

[59] Costa L, Faustino MAF, Neves MGPMS, Cunha A, Almeida A. Photodynamic inactivation of mammalian viruses and bacteriophages. Viruses 2012;4:1034–74. https://doi.org/10.3390/v4071034.

[60] Fedorenko A, Grinberg M, Orevi T, Kashtan N. Survival of the enveloped bacteriophage Phi6 (a surrogate for SARS-CoV-2) in evaporated saliva microdroplets deposited on glass surfaces. Sci Rep 2020;10:1–10. https://doi.org/10.1038/s41598-020-79625-z.

[61] Silverman AI, Boehm AB. Systematic review and meta-analysis of the persistence and disinfection of human coronaviruses and their viral surrogates in water and wastewater. Environ Sci Technol Lett 2020;7:544–53. https://doi.org/10.1021/acs.estlett.0c00313.

[62] Aquino De Carvalho N, Stachler EN, Cimabue N, Bibby K. Evaluation of Phi6 persistence and suitability as an enveloped virus surrogate. Environ Sci Technol 2017;51:8692–700. https://doi.org/10.1021/acs.est.7b01296.

[63] Whitworth C, Mu Y, Houston H, Martinez-Smith M, Noble-Wang J, Coulliette-Salmond A, Rose L. Persistence of bacteriophage Phi 6 on porous and nonporous surfaces and the potential for its use as an ebola virus or coronavirus surrogate. Appl Environ Microbiol 2020;86:1–11. https://doi.org/10.1128/AEM.01482-20.

[64] Ye Y, Ellenberg RM, Graham KE, Wigginton KR. Survivability, partitioning, and recovery of enveloped viruses in untreated municipal wastewater. Environ Sci Technol 2016;50:5077–85. https://doi.org/10.1021/acs.est.6b00876.

[65] Costa L, Tomé JPC, Neves MGPMS, Tomé AC, Cavaleiro JAS, Faustino MAF, Cunha Â, Gomes NCM, Almeida A. Evaluation of resistance development and viability recovery by a non-enveloped virus after repeated cycles of APDT. Antivir Res 2011;91:278–82. https://doi.org/10.1016/j.antiviral.2011.06.007.

[66] Bartolomeu M, Monteiro CJP, Fontes M, Neves MGPMS, Faustino MAF, Almeida A. Photodynamic inactivation of microorganisms in different water matrices: the effect of physicochemical parameters on the treatment outcome. Sci Total Environ 2023;860:160427. https://doi.org/10.1016/j.scitotenv.2022.160427.

[67] Armarego WLF, Chai CLL. Purification of laboratory chemicals; butterworth-heinemann, ed.; seventh. Oxford: Elsevier; 2013.

[68] Kollar J, Machacek M, Halaskova M, Lenco J, Kucera R, Demuth J, Rohlickova M, Hasonova K, Miletin M, Novakova V, et al. Cationic versus anionic phthalocyanines for photodynamic therapy: what a difference the charge makes. J Med Chem 2020;63:7616–32. https://doi.org/10.1021/acs.jmedchem.0c00481.